A Reliability Study with Infrared Imaging of Thermoelectric Modules under Thermal Cycling

Michael T. Barako, Woosung Park, Amy M. Marconnet, Mehdi Asheghi, and Kenneth E. Goodson
Department of Mechanical Engineering
Stanford University
440 Escondido Mall
Stanford, CA 94305
Phone: (717)339-6794
Email: mbarako@stanford.edu

ABSTRACT

Thermoelectric (TE) modules undergo performance degradation and mechanical failure due to thermal cycling. In the present study, TE modules are subjected to thermal cycling, and the thermoelectric performance is evaluated at periodic intervals. Both the thermoelectric figure of merit, *ZT*, and the individual components of *ZT* are measured at each interval. The thermopower and thermal conductivity are measured using steady state infrared microscopy, and the electrical conductivity and *ZT* are evaluated using a variation of the Harman technique. These properties are tracked over many cycles until device failure. Critical failure occurred after 45,000 thermal cycles, and the mechanical failure of the TE module is analyzed using high-resolution infrared microscopy and scanning electron microscopy. These results quantify the effect of thermal cycling on a commercial TE module performance and provide insight into the packaging of a complete TE module for reliable operation.

KEY WORDS: infrared microscopy, Harman method, thermoelectric materials, infrared failure analysis

NOMENCLATURE

A	cross-sectional area
I	electrical current
k	thermal conductivity
L	length of TE element
q	heat flow
q"	heat flux
StdDev	standard deviation
T	temperature
V	voltage
x	position along direction of conduction heat flow
ZT	thermoelectric figure of merit
Greek symbols	
α	Seebeck coefficient
ρ	electrical resistivity
σ	electrical conductivity
Subscripts	
0	at 0 cycles
E	electrical component of voltage
oc	open circuit voltage
ref	reference layer
TE	thermoelectric
TE leg	single thermoelectric leg element
T	thermal component of voltage
total	total voltage

INTRODUCTION

Thermoelectric (TE) modules are solid state devices used in the direct conversion between thermal and electrical energy. A TE module can operate in a power generation configuration where a temperature difference generates a gradient in electrical potential. This allows TE modules to generate electricity from heat sources such as combustion processes or solar irradiation. This has been proposed as an efficient method for recovering low-grade waste heat from combustion processes, such as in automobiles [1]. Alternatively, a TE module can operate as a solid state refrigerator when supplied with electrical power. This has enabled the miniaturization of refrigeration cycles and heat pumps, such as those used in electronics cooling [2].

A TE module consists of many semiconductor legs connected electrically in series and thermally in parallel. The legs alternate between n- and p-type thermoelectric materials (typically Bi_2Te_3-alloys for modern commercial modules). Often these legs are soldered to copper interconnects, which creates a thermally conductive but mechanically brittle metallic bond. The inherently large temperature gradients across TE modules and the large number of thermal cycles during operation lead to performance degradation and device failure at these interfaces [3]. Thermomechanical stresses at the leg-interconnect solder interfaces arise due to the mismatch of the coefficient of thermal expansion between the bonded materials and the solder. In addition to large individual temperature gradients, thermal cycling also reduces device performance and leads to device failure [4, 5]. Thermal cycling of TE modules is common for both refrigeration and electricity generation applications. Fluctuations in the temperature gradients lead to stresses which create microcracks at the brittle solder interfaces and can also lead to material changes in the semiconductor legs. It is therefore important to understand and quantify the effects of thermal cycling on the performance of a TE module.

The standard TE performance metric is the nondimensional figure of merit, *ZT*, which depends on the thermal conductivity k, the electrical conductivity σ, and the Seebeck coefficient α.

$$Z\bar{T} = \frac{\sigma\alpha^2}{k}\bar{T} \qquad (1)$$

where $\bar{T}$ is the average temperature of the module (taken as the mean temperature of the hot and cold plates). In this work, we measure both the individual components of *ZT* and the value of *ZT* directly. The thermal conductivity and Seebeck coefficient of the TE module are measured using a steady state infrared thermometry technique which measures two-

dimensional cross-sectional temperature maps of the TE module. The electrical conductivity is determined using a DC electrical technique by sourcing current and extracting the electrical component of the voltage drop across the TE module. *ZT* is directly computed using the Harman technique.

The effects of thermal cycling are examined by imposing a square wave voltage across the TE module and measuring the properties at predetermined intervals. One side of the module is exposed to ambient convection and heats to +146°C and cools to -20°C over a period of 60 seconds during thermal cycling. The other side of the module is maintained at isothermal conditions (23°C) using a copper heat exchanger. The module properties are measured using the aforementioned combination of techniques at periodic cycling intervals.

EXPERIMENTAL

Thermal Cycling

The TE module is clamped to a copper heat sink on one side with a thin layer of thermal grease. The other side is exposed to ambient natural convection conditions. Moderate compressive pressure is maintained during all thermal cycling to reproduce the operating conditions of an actual device. A voltage source applies a square wave signal across the TE module between +2.3V and -2.3V to induce a temperature gradient across the module.

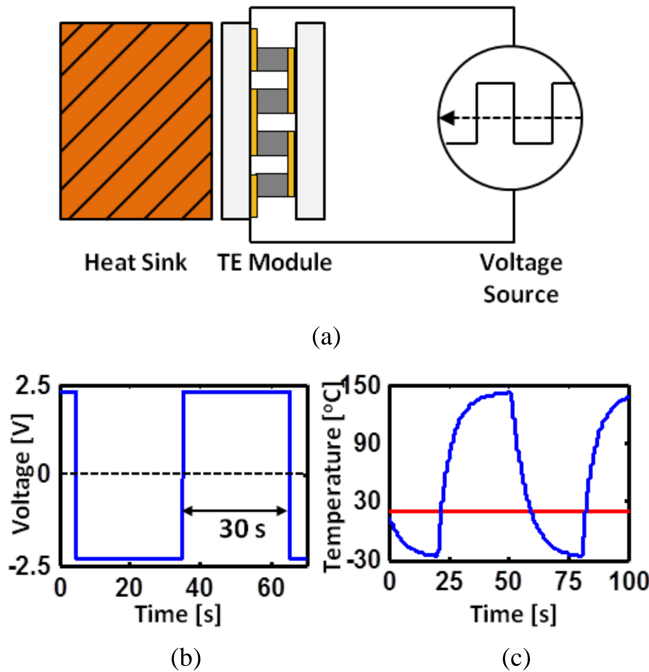

Fig. 1: (a) The TE module is placed with one side against a copper heat sink which is isothermal at 23°C. The module is clamped (not shown) to the heat sink. This provides moderate compressive pressure to more closely represent the mechanical boundary conditions of a real application. (b) A square wave voltage is applied at V_{pp} = +/- 2.3V with a period of 60 seconds. (c) This voltage induces a temperature profile where the open air side of the TE module (blue) oscillates between 146°C and -20°C while the isothermal side (red) remains near 23°C.

This is the maximum voltage rating for this particular device, and it causes the convective side of the TE module to oscillate between +146°C and -20°C. The width of each square pulse is 30 seconds, which allows the device to reach 95% of the steady state temperature before Joule heating becomes significant. The large thermal mass of the heat sink maintains the heat sink surface temperature at ~23°C over the duration of a complete thermal cycle. At predetermined intervals, the thermal cycling is stopped and the thermoelectric properties of the TE module are measured. The structure is clamped together to apply uniform compressive pressure to better represent the mechanical boundary conditions under actual operating conditions. This constrains the thermal expansion, which leads to the formation of thermomechanical stresses in the module and at the interfaces.

This testing condition utilizes a Peltier cooling configuration rather than a power generation configuration. However, the supplied voltage serves only to establish a temperature gradient and to impose stresses on the module. This cycling configuration is assumed to be representative of thermomechanical stresses in systems under both Peltier cooling operation and power generation operation. Electromigration of molecular species due to the presence of an electric field and charge transport is another primary source of performance reduction over the life cycle of a TE device. This specific effect is not independently examined in the present work.

Infrared Microscopy

Infrared (IR) microscopy is a non-invasive temperature measurement technique that generates a high resolution two-dimensional temperature map. This temperature map is used to determine the thermal conductivity and Seebeck coefficient of the module. The IR microscope (Quantum Focus Instruments) provides a temperature resolution up to 0.1°C and a spatial resolution up to the diffraction limit of 2μm. This temperature profile is used to accurately measure the temperature difference across the individual TE elements. Simultaneous measurements of the open-circuit voltage and this temperature difference yields the Seebeck coefficient of the module.

The thermal conductivity is determined from this IR imaging using a comparative technique where reference layers are placed in thermal series with the TE module. Fused silica was chosen as the reference layer due to its stable thermal conductivity of k_{ref} = 1.4 W/m/K over a wide range of temperatures. A reference layer is placed on both sides of the TE module. One side of this stack is then heated via external electrical heater and the other side is maintained at a cold temperature using a chilled water heat exchanger. This temperature difference causes heat to conduct through the stack. Since the reference layers are prepared with the same cross-sectional total area as the TE module, heat conducted through the stack is approximately one-dimensional. Once steady state conditions are reached, the IR microscope measures a two-dimensional temperature map along the length of the stack. The temperature gradient in each layer is governed by Fourier's Law.

$$q = q''A = kA\frac{dT}{dx} \tag{2}$$

Since all of the layers are in thermal series and we can neglect convective and radiative effects, the same quantity of heat conducts through the reference layers and also the TE module. The use of two reference layers permits the quantification of heat losses by convection and radiation. The difference between the heat conducted through the hot-side reference layer and the cold-side reference layer corresponds to the heat lost in the stack. These two values for heat flux also serve as an upper and lower bound in estimating the heat conducting through the TE module. Since these two values were calculated to differ by less than 10%, it is assumed that conduction is the primary mode of heat transfer for the analysis. The temperature gradient is simultaneously measured in the reference layers and in the TE legs. Since heat flow is one-dimensional, the two-dimensional temperature map is averaged in the direction perpendicular to the heat flux to reduce the effects of experimental noise on the temperature profile.

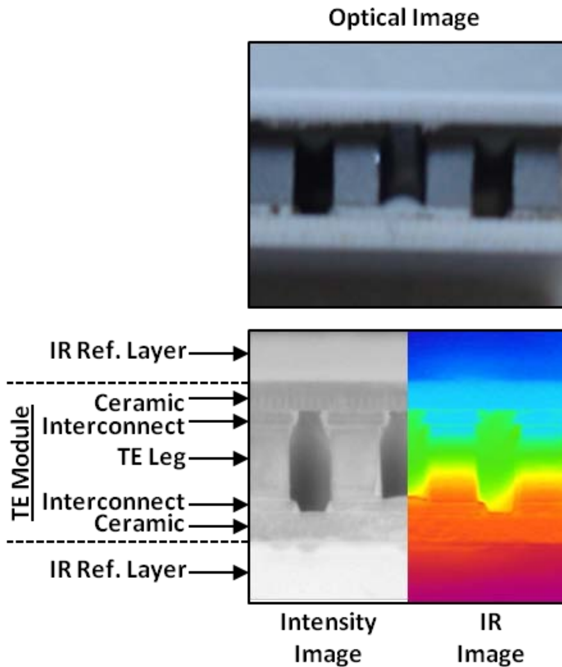

Fig. 2: (Top) Optical microscope image of TE module highlighting the ceramic supports, copper interconnects, and semiconductor legs. (Bottom) Infrared image of the cross-section of a TE module. The grayscale intensity image (left) shows the radiation intensity while the false color image (right) indicates the spatially-varying temperature profile. Fused silica reference layers are placed on both sides of the TE module as reference layers for thermal measurements. As heat conducts through the structure, a temperature profile is set up and the relative magnitude of the temperature gradients and jumps relate to the thermal conductivity and thermal boundary resistances, respectively.

This yields a one-dimensional temperature profile along the length of the conduction heat flux vector. Using Fourier's Law, the thermal conductivity of each TE leg is calculated by comparing the heat conducted through the reference layers to the temperature gradient and area of the TE leg.

$$\frac{k_{TE}}{k_{ref}} = \frac{A_{ref}\left(\frac{dT}{dx}\right)_{ref}}{A_{TE}\left(\frac{dT}{dx}\right)_{TE}} \quad (3)$$

In addition, the Seebeck coefficient is calculated by simultaneously measuring the open-circuit DC voltage while measuring the temperature profile using the IR microscope. This allows for a more accurate temperature measurement compared to external thermocouples. Specifically, we can directly measure temperature across the TE elements inside of the module for computing the Seebeck coefficient independent of the temperature jump at the boundary. By simultaneously measuring open circuit voltage ΔV_{oc} and the temperature drop across the TE legs ΔT, the Seebeck coefficient of the module is

$$\alpha = \lim_{\Delta T \to 0} \frac{\Delta V_{OC}}{\Delta T}. \quad (4)$$

In contrast, thermocouples require physical contact to the modules and can be difficult to precisely locate on the TE module. Thermocouples also provide a parallel conduction pathway which can affect the accuracy of the measured temperature. Through IR imaging we directly probe the temperature at the interconnect surface without affecting the measured value.

Infrared imaging also allows for high spatial resolution detection of material defects by observing anomalies in the thermal signature of a device that is conducting heat. TE modules tend to fail at the interconnect-leg interface due to thermal cycling and the consequential thermomechanical stresses caused by large temperature gradients [6].

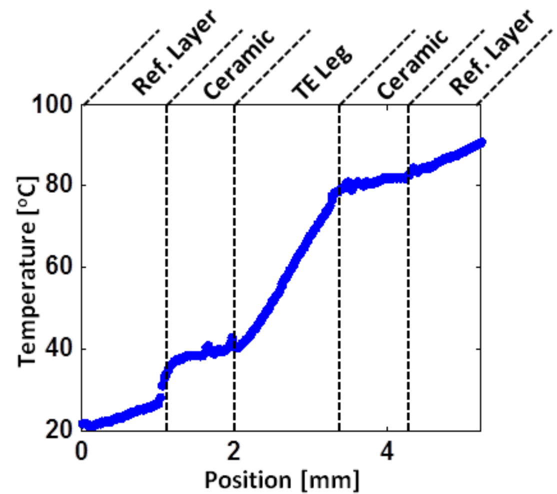

Fig. 3: Cross-sectional temperature profile of a TE module sandwiched between two fused silica reference layers. The slope of each region is determined using a linear least-squares fit. The temperature drop across the TE leg is used in determining both the thermal conductivity and the Seebeck coefficient of the module. The ceramic layers also include the copper interconnect. Noise in the ceramic layers is due to the presence of interfaces and the surface roughness of the soldered connection.

Cracks and physical damage may be difficult to detect optically but are well-defined in their thermal signature when passing heat across the damaged region. A crack behaves as an interface with a high thermal resistance. This appears on the IR image in the form of a hotspot and a corresponding temperature jump [7]. Nonuniformities in the 1D temperature profile may also indicate changes at the atomic level, including species migration and material degradation. By imaging in the infrared spectrum with a spatial resolution up to the diffraction limit (2μm) it is possible to detect material changes and device failure modes that are difficult to observe optically. We can also detect cracks at the interconnects by looking for changes in the thermal boundary resistance at each interface.

Harman Method

The Harman Method is used to determine the electrical resistivity and TE figure of merit for the module [8]. A DC current source (Keithley 6221) connected to the TE module applies a 10mA DC current, resulting in a voltage across the TE module which is detected by a voltmeter (HP 3458A). This voltage has two components: (1) electrical due to the current flowing through a finite resistance, and (2) thermoelectrical due to the temperature difference across the module. The 10mA DC current is applied for 70 seconds, which is sufficient time for the system to reach thermal steady state, as determined by the stability of the voltage. The current source was then turned off. This eliminates the electrical contribution of the voltage, leaving only the thermoelectric component. The TE module was then allowed to cool for 60 more seconds, during which time the TE module reached thermal equilibrium and the thermoelectric voltage decayed to zero.

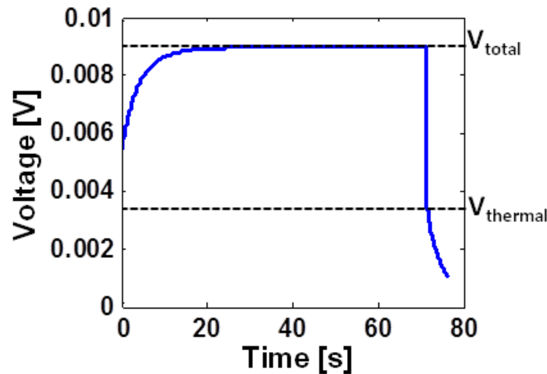

Fig. 4: Example Harman method voltage trace for applied current of 10 mA for 70 s. V_{total} consists of the electrical and thermoelectrical voltage, while $V_{thermal}$ is the thermoelectric voltage and is the voltage immediately after the current source is turned off. The transient regions (t<30 s, t>70 s) correspond to the thermal response time while the thermal component of voltage reaches steady state.

This was repeated at least ten times and the results were averaged to ensure an accurate analysis. The total voltage is measured just before the current source is stopped and the thermoelectric voltage is measured just after the removal of the current. The ability to detect the thermoelectric voltage is limited by the temporal resolution of the voltmeter. The electrical contribution to voltage is the difference between these two values. Using Ohm's Law, the electrical resistance of the module can be calculated.

Harman *et al*. [8] present the following definitions based on first principles for the individual thermoelectric properties:

$$\rho = \frac{V_E A}{IL} \tag{5}$$

$$\alpha = \frac{V_T}{\Delta T} \tag{6}$$

$$k = \frac{\alpha I \bar{T} L}{\Delta T A_{TE}} \tag{7}$$

These terms are substituted into Eq. 1 to calculate *ZT* from measured properties. The TE figure of merit *ZT* is calculated from the same voltage trace [8]:

$$Z\bar{T} = \frac{V_T}{V_E} \tag{8}$$

These calculations are valid for small temperature differences across the module, which is proportional to the current supplied. For these measurements with an applied current of 10mA current, the temperature difference is <1°C.

RESULTS

Thermoelectric Module Performance

For a constant applied voltage (+/- 2.3 V), the resulting temperature range during thermal cycling decreased over time, while the thermal time constant of the TE module dramatically increased with cycles. Initially, with V_{pp} = +/- 2.3VDC, the temperature range was observed to be 146°C/-20°C. At ~45,000 cycles, the TE module broke, as indicated by the substantially reduced temperature range for the same voltage input signal. At this point, the temperature range over a full cycle oscillated between 40°C and 20°C. This sudden degradation in ZT is due primarily to interface fracture, which increased the electrical resistivity by several orders of magnitude. We were able to detect the formation of cracks at the leg-interconnect junction using the IR microscope that were not optically visible.

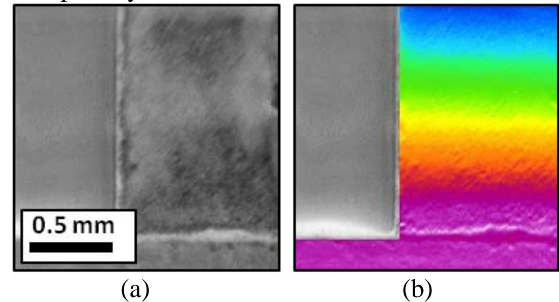

(a) (b)

Fig. 5: (a) Optical and (b) infrared image of the interface between a TE leg and a copper interconnect. As heat conducts through the interconnect and the TE leg, we can identify damage by examining nonuniformities in the temperature map. This image was taken prior to thermal cycling. As a result, the temperature map is smooth and linear, indicating an undamaged thermoelectric material.

These cracks appear as bright lines on the IR temperature map. In addition, we found that many of the legs now have non-parallel isotherms, indicating that heat is no longer flowing uniformly through the TE material. Baseline IR temperature maps were measured before cycling to verify the uniformity associated with unstressed TE elements.

After 45,000 cycles, there were multiple TE legs that exhibited thermal signatures that are characteristic of mechanical damage. Often the nonuniform temperature distribution was accompanied by a partial crack at the soldered interface. As a result, the thermal resistance becomes very large across the region with the crack compared to the region that maintained mechanical integrity. Consequently, heat no longer conducts equally at the boundaries of the leg and the temperature distribution within the leg changes to match the new boundary conditions. This conclusion was verified using scanning electron microscopy.

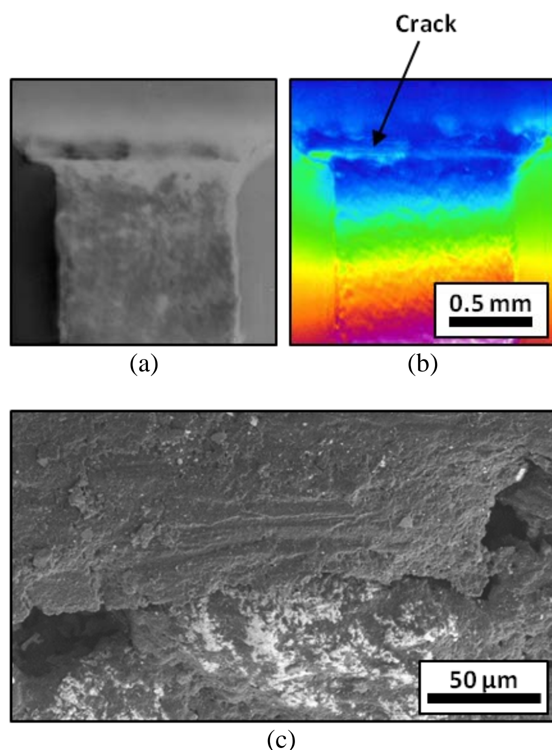

Fig. 6: (a) Optical and (b) infrared image of a damaged solder interface between the interconnect and TE leg. Here we see a crack on the left half of the interface. The mechanical damage is not apparent in the optical image alone. However, the temperature nonuniformity and non-parallel isotherms in the IR imaging allows rapid assessment of the extent of thermomechanical damage at the brittle solder bonds. (c) SEM micrograph showing the propagation of a microcrack in the solder interface.

Thermoelectric Figure of Merit

The TE figure of merit is calculated directly using the Harman method at predetermined intervals. The baseline measurement yielded a figure of merit value of $ZT = 0.6244$ (StdDev = 0.0026). Thermal performance degraded steadily during the first 10,000 cycles. Between 10,000 and 45,000 cycles, performance drops substantially, eventually leading to complete device failure. Device failure was determined when the TE module could sustain 2.3V but the current became very small (corresponding to high electrical resistance), yielding sizable reductions in the temperature range of the device. While the thermal voltage dropped slightly after failure, the electrical voltage increased by more than an order of magnitude. This is indicative of a large contact resistance being introduced into the system.

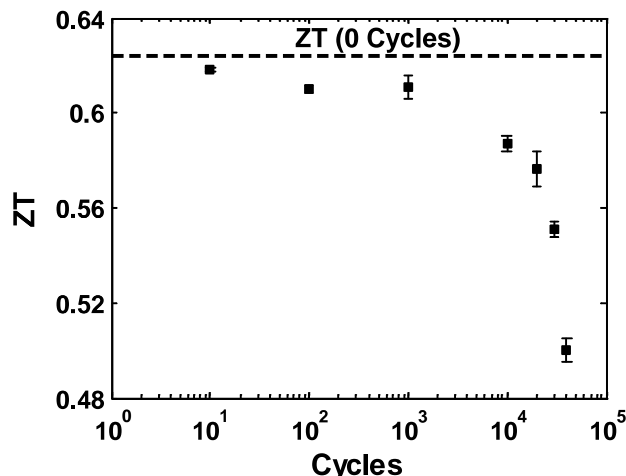

Fig. 7: Effect of thermal cycling on the TE figure of merit as measured using the Harman method. These data indicate TE performance up to critical failure. Error bars indicate one standard deviation from the mean.

The reduction in *ZT* is the first major indicator of reduced TE module performance under cycling. The reduction is most dramatic after 10,000 cycles as the device begins to break down mechanically. At the point of critical failure (45,000 cycles), *ZT* was reduced to 3.16% of the baseline value to a value of $ZT = 0.0197$. We next investigate the individual components that comprise *ZT* to get a better understanding of the degree in which each component contributes to this performance reduction.

Individual Thermoelectric Properties

During each measurement interval, the electrical conductivity, thermal conductivity, and Seebeck coefficient are each calculated separately. IR imaging is used to obtain the thermal conductivity and the Seebeck coefficient, while the Harman method is used to measure the electrical conductivity. This allows tracking of the individual properties over time. A baseline value of each property was measured prior to cycling, in order to establish the values for the unstressed TE module. Subsequent measurements after cycling were considered relative to this baseline.

The electrical resistance of the module is found to be the most dynamic individual thermoelectric property with cycling. The resistance monotonically increased with cycles, which we hypothesize is due to the increased contact resistance at each microcrack. As thermal cycling induces microscopic damage in the current path, this introduces an additional electrical resistance due to contact across the crack. The resistance increased from $R = 0.5511\ \Omega$ (StdDev = 0.0001) prior to thermal cycling up to $R = 0.6748\ \Omega$ (StdDev = 0.0013)

after 40,000 cycles. This is a 22% increase in electrical resistance. At 45,000 cycles, when the device fails at a leg-interconnect interface, a large single contact resistance is introduced, increasing the electrical resistance by a factor of ~30 to R = 16.22 Ω (StdDev = 0.012).

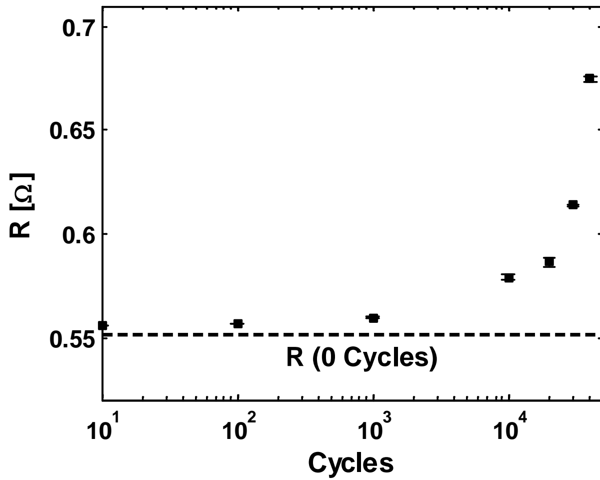

Fig. 8: Electrical resistance increases with the number of thermal cycles. This is attributed primarily to the formation of microcracks which increase the contact resistance. Error bars indicate one standard deviation from the mean and are approximately the size of the marker.

The thermal conductivity is measured for two adjacent legs to ensure that we considered both n- and p-type legs. The module is placed between the two reference layers and heat is conducted through the sample. The heat flux was measured in each reference layer and compared to ensure that we can ignore the effects of convection and radiation. In each of these measurements, the heat flux discrepancy was less than 10%. A temperature map was measured for a range of different hot-side temperatures from 50°C to 130°C. For each heat flux conducted through the sample, the temperature gradient in the two adjacent TE legs was measured. The same two TE legs are measured at each cycling interval. The thermal conductivity increased minimally during cycling by a value less than the uncertainty of the measurement. The measured values are k = 0.840 W/m/K (StdDev = 0.136) and k = 0.821 (StdDev = 0.124) for each of the two measured legs.

The Seebeck coefficient is determined by measuring the voltage output of the TE module while varying the heat flux through the sample. Once the module reaches equilibrium with a stable open circuit voltage, an IR temperature map and TE voltage are simultaneously recorded to compute the Seebeck coefficient. The Seebeck coefficient remains relatively stable throughout the duration of the thermal cycling.

The Seebeck coefficient increases with temperature over the measurement temperature domain of 30°C to 70°C. For each measured Seebeck value, the mean temperature was measured between the hot side and cold side of the TE legs at the interconnect interface (inside of the module).

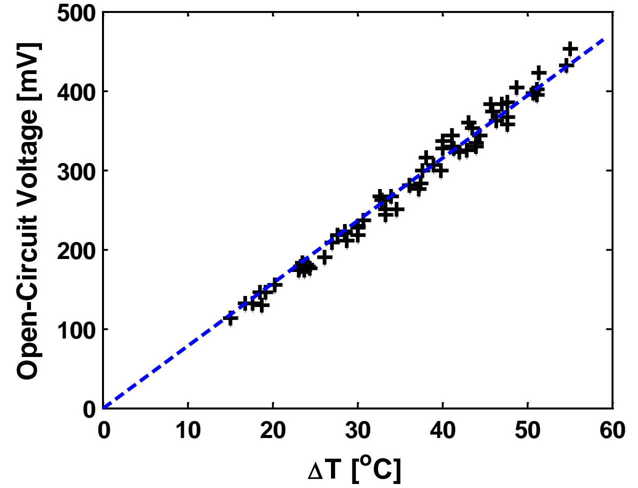

Fig. 9: Open circuit TE module voltage vs. temperature difference across the TE module. The slope of this plot yields the Seebeck coefficient. During thermal cycling, this data continues to fall along the same line, indicating that the Seebeck coefficient is stable. These data points include all measurements taken at each cycling interval prior to device failure from 0 to 40,000 cycles.

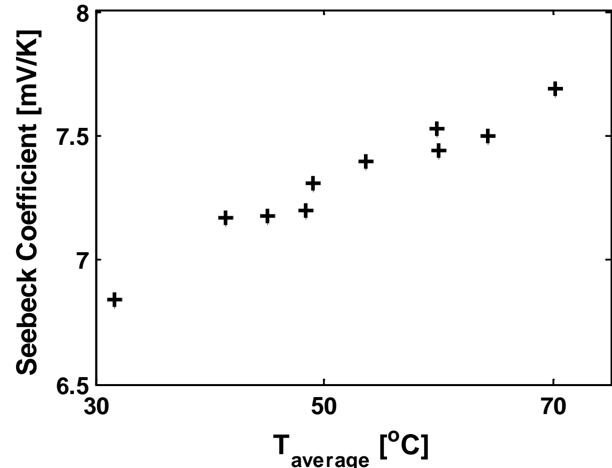

Fig. 10: Seebeck coefficient vs. mean TE module temperature. The mean temperature of the TE module is taken as the mean temperature of the inner side of the hot- and cold-side ceramic plates. Over the range of measured temperatures, the Seebeck coefficient increases monotonically with temperature from 30°C to 70°C. Data shown is the baseline measurement at 0 cycles, but this trend is consistent at each cycling interval.

The figure of merit ZT depends linearly on the electrical conductivity as shown in Eq. 1. At 45,000 cycles, we find that the most significant thermoelectric property change is the decrease in electrical conductivity (by a factor of 29.44). Therefore, we expect ZT to decrease to 3.40% of the baseline value due to electrical conductivity alone. The Harman method was already used to directly compute ZT = 0.0197, or 3.16% of the baseline value at 45,000 cycles. This indicates that at the point of device failure, ZT is reduced to 3.40% of the baseline value due to the decrease in electrical

conductivity and the remaining 0.24% reduction is due to the increase in thermal conductivity of the legs.

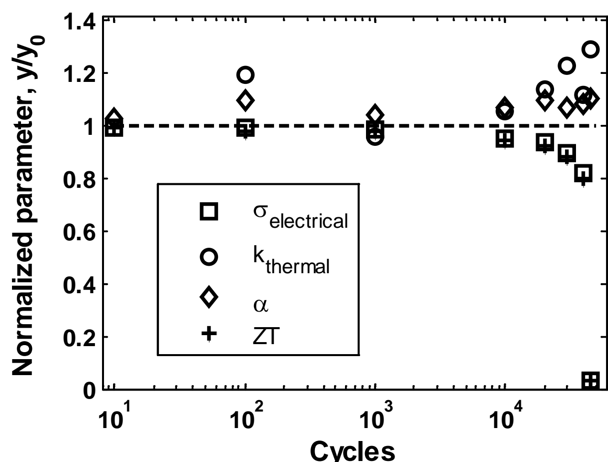

Fig. 11: Normalized thermoelectric properties vs. number of thermal cycles. All values are normalized relative to the baseline value measured at 0 cycles. This data represents measurement intervals in the thermal cycling from 0 cycles through the point of device failure at 45,000 cycles. Thermal conductivity increases by ~20% over the baseline value. The electrical conductivity demonstrates the largest deviation with thermal cycling and decreases by a factor of ~30 after 45,000 cycles. The Seebeck coefficient remains stable during the lifetime of the device. Consequently, *ZT* drops to 3.16% of the original value.

CONCLUDING REMARKS

Thermoelectric performance degrades with thermal cycling as indicated by a continuous reduction of the figure of merit *ZT* with cycles and ultimately by device failure around 45,000 cycles. This was indicated by the reduced operating temperature range during thermal cycling, the increase of electrical resistance by a factor of ~30, and the identification of microscopic cracks formed at the TE leg-interconnect interface by IR imaging. Crack formation at the interfaces led to this dramatic increase in electrical resistance due to interfacial contact. Ongoing work to address these design issues focuses the use of nanostructured thermal interface materials to alleviate these interface thermomechanical stresses while providing good thermal and electrical conduction across the interface.

ACKNOWLEDGEMENTS

The authors gratefully acknowledge financial support from the NSF/DOE Partnership on Thermoelectric Devices for Vehicle Applications (Grant No. 1048796), the National Science Foundation Graduate Research Fellowship program, the Stanford Graduate Fellowship program, and the Korea Institute of Energy Technology Evaluation and Planning Fellowship program. The SEM micrographs are courtesy of Yuan Gao.

REFERENCES

[1] K. Zorbas, E. Hatzikraniotis, and K. Paraskevopoulos, "Power and Efficiency calculation in commercial TEG and application in wasted heat recovery in automobile," 2007.

[2] I. Chowdhury, R. Prasher, K. Lofgreen, G. Chrysler, S. Narasimhan, R. Mahajan, D. Koester, R. Alley, and R. Venkatasubramanian, "On-chip cooling by superlattice-based thin-film thermoelectrics," *Nat Nanotechnol,* vol. 4, pp. 235-8, Apr 2009.

[3] E. Hatzikraniotis, K. T. Zorbas, I. Samaras, T. Kyratsi, and K. M. Paraskevopoulos, "Efficiency Study of a Commercial Thermoelectric Power Generator (TEG) Under Thermal Cycling," *Journal of Electronic Materials,* vol. 39, pp. 2112-2116, 2009.

[4] Y. Gao, A. M. Marconnet, M. A. Panzer, S. LeBlanc, S. Dogbe, Y. Ezzahri, A. Shakouri, and K. E. Goodson, "Nanostructured Interfaces for Thermoelectrics," *Journal of Electronic Materials,* vol. 39, pp. 1456-1462, 2010.

[5] Y. Hori, D. Kusano, T. Ito, and K. Izumi, "Analysis on thermo-mechanical stress of thermoelectric module," in *Thermoelectrics, 1999. Eighteenth International Conference on*, 2000, pp. 328-331.

[6] D. M. Rowe and G. Min, "Evaluation of Thermoelectric Modules for Power Generation," *Journal of Power Sources,* vol. 73, pp. 193-198, 1998.

[7] R. G. de Villoria, N. Yamamoto, A. Miravete, and B. L. Wardle, "Multi-physics damage sensing in nano-engineered structural composites," *Nanotechnology,* vol. 22, p. 185502, May 6 2011.

[8] T. C. Harman, J. H. Carn, and M. J. Logan, "Measurement of Thermal Conductivity by Utilization of the Peltier Effect," *Journal of Applied Physics,* vol. 30, 1959.